JOURNAL OF SOLID STATE CHEMISTRY 59, 23–41 (1985)

Magnetic Phase Diagrams and Helical Magnetic Phases in $M_xNi_{1-x}Br_2$ (M = Fe, Mn): A Neutron Diffraction and Magneto-optical Study

MARTIN W. MOORE AND PETER DAY

Inorganic Chemistry Laboratory, Oxford University, South Parks Road, Oxford OX1 3QR, England

Received August 24, 1984; in revised form December 26, 1984

Below T_N = 44 K, $NiBr_2$ orders as an easy-plane antiferromagnet, but at $T_{IC} \sim 23$ K it undergoes a transition to a helimagnetic phase whose propagation vector, τ, increases smoothly to a limiting value [0.027,0.027,0] at 4.2 K. The magnetic order in $NiBr_2$ and $M_xNi_{1-x}Br_2$ (M = Fe, Mn) is investigated by single-crystal neutron diffraction. In $Fe_xNi_{1-x}Br_2$ τ changes from the [110] to [100] direction at 3.7(17)% Fe. Its magnitude, and T_{IC}, remain constant up to 9.9(14)% Fe, but above this concentration a collinear, easy-axis structure is stable at all temperatures below T_N, which decreases towards the value of 11 K in $FeBr_2$. Doping 2.9% Mn^{2+} into $NiBr_2$ decreases T_{IC} slightly, in the manner previously observed for diamagnetic dopants. Refinement of powder X-ray diffraction profiles show the lattice distortions in the doped materials to be small, while the structures of some $Fe_xNi_{1-x}Br_2$ samples are confirmed by refinement of the powder neutron diffraction profiles. The temperature and field dependence of hot and cold exciton–magnon combination bands in the optical absorption spectra of Fe^{2+}- and Mn^{2+}-doped crystals give additional information about magnetic order. The magnetic behaviour is interpreted in terms of perturbations of the exchange constants $J_{1,2,3}$, and J' and the anisotropy constant D.

1. Introduction

The magnetic behaviour of $NiBr_2$ is unique among the layer transition metal dihalides, and possibly among all insulating magnetic compounds. Early susceptibility measurements (*1, 2*) indicated that below T_N = 52 K, it orders antiferromagnetically with a metamagnetic structure similar to $NiCl_2$. However, more recent single-crystal neutron diffraction experiments (*3, 4*) have shown that, below $T_{IC} \sim 23$ K, it undergoes a transition to a helimagnetic phase characterised by a propagation vector τ in the [110] direction. Moreover τ increases with decreasing temperature, reaching a maximum value [0.027,0.027,0] at 4.2 K (*3*). Single-crystal susceptibility measurements (*3*) also demonstrated that whereas the susceptibility along [001] increases smoothly below T_N, perpendicular to the c axis it exhibits a discontinuity at about 22 K, thus confirming that the transition involves a rearrangement of the spin orientations within the *ab* planes.

The helimagnetic phase arises from a balance among the intraplanar exchange constants J_1, J_2, and J_3. Rastelli *et al.* (*5*) have shown how helical magnetic structures may be stabilized in two-dimensional hexagonal

0022-4596/85 $3.00

lattices of localized moments with planar anisotropy, but no theory is available at present to explain the temperature dependence of τ and the commensurate–incommensurate phase transition. The Rastelli model indicates the relative stability of two possible collinear phases (ferromagnetic I and antiferromagnetic II), as well as two helical phases ([100] III, and [110] IV) as a function of ratios between the various exchange constants $j_n = z_n J_n / z_1 J_1$, where z is the number of neighbours of each type.

Neutron diffraction and susceptibility (*7*) measurements on single crystals of $NiBr_2$ under hydrostatic pressure show that T_{IC} decreases linearly by about 10.5% per kbar. Day and Vettier (*6*) also observed that τ decreases in magnitude with increasing pressure, and reasoned that if this is due to changes in $J_{1,2,3}$ then the decrease in τ with increasing temperature cannot arise from changes in $J_{1,2,3}$ due to lattice expansion. Attempts have also been made to perturb the balance of the intraplanar exchange coupling by chemical doping. Neutron diffraction experiments on a single crystal containing 8-mole% Zn^{2+} (*8*) showed that in zero field T_{IC} is reduced to 21 K and the helical propagation vector direction within the **a*b*** plane becomes disordered.

Both low- and high-resolution absorption spectra of single crystals of pure $NiBr_2$, down to liquid helium temperature, have been reported. Interest has centered on the region 5800 to 6100 Å where a weak but highly structured band system is seen at low temperature (*10, 11*). There is no trace of a corresponding band system in the spectrum of $NiCl_2$ (*12*), so it is believed to be connected with the peculiar magnetic structure of $NiBr_2$.

In particular, three electric dipole transitions at the electronic origin of the phonon sideband structure have been assigned to exciton–magnon transitions. A pair of sharp cold bands (wavelength 6080.0 and 6082.9 Å at 4.2 K) move together and decrease in intensity with increasing temperature. They converge and their intensity falls sharply to zero in a manner characteristic of a first-order phase transition at the transition temperature T_{IC} found from neutron scattering and susceptibility measurements (*10*). Thus, they only appear when the crystal is in the helimagnetic phase so their temperature and field dependence serves to map the magnetic phase diagram in the (H_{ab},T) plane (*10*). A broad, asymmetric hot band centred at 6075 Å dominates this region of the spectrum above about 12 K (*10, 13*). It persists up to the three-dimensional ordering temperature, T_N, and appears to arise from a ferromagnetic component of the exchange coupling within the *ab* planes. In a 7.7 mole% Zn^{2+} crystal, the H_{ab},T) phase diagram, obtained in the same way as for pure $NiBr_2$ revealed that the stability region of the helical phase decreases with increasing concentration of Zn^{2+} ions (*8*).

Pollard *et al.* (*14*) have reported the results of Mossbauer spectroscopy on nickel dihalides doped with $^{57}Fe^{2+}$ ions. The measurements performed on a single crystal of $NiBr_2$ containing 0.63 mole% Fe^{2+} showed that in the collinear phase below $T_N \sim 46$ K the Fe^{2+} moments are directed along the hexagonal [110] directions. A change in the orientation of the net magnetisation was observed at low temperature, but neither the transition temperature nor the nature of the low-temperature magnetic phase could be identified.

The object of the work described in this paper is to investigate how the magnetic structure of $NiBr_2$ is perturbed by partial substitution of Fe^{2+} and Mn^{2+}. $FeBr_2$ is an easy-axis metamagnet with the CdI_2 structure. The large axial single ion anisotropy directs the Fe^{2+} moments parallel to the c axis. The $Fe_xNi_{1-x}Br_2$ system is expected to have an easy-axis magnetic structure above a limiting value of x, but the effect upon the modulated spin structure of $NiBr_2$

at lower concentrations of Fe^{2+} ions will depend upon how the moments of the latter orientate themselves. A structural phase transition to the CdI_2 layer structure may also be expected to take place. $MnBr_2$ has complex noncollinear magnetic phases. However, it is characterised by a small ferromagnetic nearest-neighbour intraplanar exchange constant J_1 and a small planar anisotropy constant D. The system $Mn_xNi_{1-x}Br_2$ may thus behave in a manner similar to $Zn_xNi_{1-x}Br_2$. The magnetic structure of the doped crystals is investigated by neutron diffraction as well as by observing the exciton–magnon combination bands in the optical absorption spectra.

2. Experimental

2.1. Preparation and Handling of Materials

Nickel(II) bromide (Alfa Inorganics, purity 99.9%) was purified by sublimation in a silica tube at 10^{-5} mbar. Drying at 200°C was followed by two successive sublimations at 580°C.

Iron(II) bromide and manganese(II) bromide were prepared using the reaction (*15*)

$$M(s) + 2HBr(g) \xrightarrow[\sim 900°C\ (M = Mn)]{\sim 800°C\ (M = Fe)} MBr_2(s) + H_2(g).$$

Iron powder (purity 99.99%) was obtained from Goodfellow Metals. The MBr_2 product was zone-refined using the Bridgman technique. $MnBr_2$ was prepared by a similar technique using manganese flake (Johnson Matthey Chemicals, Ltd. "Specpure"). Purification was by sublimation at 500°C.

Crystals were grown in silica ampoules by the Bridgman–Stockbarger method using Metals Research and Crystalox furnaces. Melting points of the solid solutions, found by premelting in a muffle furnace, were close to a linear function of dopant mole fraction indicating formation of nearly ideal solid solutions.

Samples from the boules were analysed by atomic absorption spectroscopy and individual crystals used during the experiments were analysed independently. The lattice parameters were also measured at room temperature by X-ray powder diffraction and at 4.2 K by neutron powder diffraction.

Samples for powder neutron diffraction were prepared by lowering ampoules containing the appropriate proportions of pure starting materials very rapidly through the Bridgman furnace [10 mm hr^{-1}]. These were then powdered and stored in sealed vanadium cans, in an atmosphere of helium gas.

2.2. Diffraction Measurements

X-Ray powder diffraction profiles were recorded using a Philips PW 1720 diffractometer.

Neutron powder diffraction profiles were recorded on the Curran diffractometer at AERE Harwell using neutrons of wavelength 1.37 Å from a germanium monochromator. The samples were contained in vanadium cans 40 mm in height, of various diameters, and were cooled to 4.2 K in a TBT liquid helium cryostat. Single-crystal neutron diffraction was measured using the Mk VI channel 2 diffractometer at AERE Harwell (wavelength 1.09 Å) with a CT 14 liquid helium cryostat and the D15 instrument at the Institut Laue–Langevin, Grenoble (1.17 Å) with a top-loading "orange" cryostat.

Single-crystal diffraction experiments were also performed at the ILL using the D16 diffractometer in the 2-circle mode. This machine operates on a cold source guide tube, providing neutrons of wavelength 4.52 Å from a pyrolytic graphite monochromator. A multidetector consisting of 1024 individual ^3He detectors (64 wires spaced at 2.5 mm in one dimension, 16 wires at 5 mm in the other) allows very rapid data collection.

All single crystals were wrapped in aluminium foil and glued to aluminium mounting pins after alignment. The crystals were oriented either in the (*h0l*) scattering plane, using 006_N and 300_N reflections, or in the (*hhl*) scattering plane, using 006_N and 110_N reflections.

2.3. *Optical Measurements*

Unpolarised absorption spectra were recorded using a high-resolution McPherson RS10 spectrophotometer. The 1-m Czerny–Turner scanning monochromator, with prism predisperser, gave a band pass of 0.3 cm^{-1}. The sample was mounted in an Oxford Instruments CF100 continuous-flow helium cryostat.

Magneto-optical studies were performed using a Thor Cryogenics superconducting magnet, providing fields up to 5 T. Sample temperature can be adjusted by means of a heater wired to a Type 3011 II controller. The spectrometer was operated in the log single beam mode.

3. Results

3.1. *Powder Diffraction*

X-Ray powder diffraction profiles were used to refine the lattice parameters by least-squares fitting the measured 2θ values of about 20 reflections. The results presented in Table I refer to the chemical hexagonal cells of the $CdCl_2$ ($R\bar{3}m$) and CdI_2 ($P\bar{3}m$) structures. The measured parameters of $FeBr_2$ and $MnBr_2$ are included for comparison.

The values of a_0 and c_0 increase slightly with increasing concentration of Fe^{2+} though the phase containing 41-mole% Fe^{2+} shows values of a_0 and c_0 less than 2% larger than those of $NiBr_2$. A transition to the CdI_2 structure of $FeBr_2$ occurs between 41 and 72 mole% Fe^{2+}. The increase in a_0 and c_0 is rather more rapid with increasing concentration of Mn^{2+}, so that samples containing 3.3 mole% Mn^{2+} and 41 mole% Fe^{2+} exhibit similar lattice expansions. In $NiBr_2$ and $FeBr_2$ there are slight compressions in the axial ratio at room temperature, while $MnBr_2$ shows a slight trigonal elongation. The mixed materials have intermediate axial ratios. In addition, the values determined from the 4.2 K powder neutron diffraction profiles of samples with 0, 8 and 30 mole% Fe^{2+} are the same as those measured at room temperature, within the error limits, indicating that magnetostrictive effects within the magnetically ordered phases are negligible.

TABLE I

REFINED LATTICE PARAMETERS FROM X-RAY POWDER DIFFRACTION PROFILES OF DOPED $NiBr_2$ SAMPLES (ROOM TEMPERATURE) WITH PURE PHASES FOR COMPARISON

Composition	a_0 (Å)	c_0 (Å)	Space group
$NiBr_2$	3.648(3)	18.39(1)	$R\bar{3}m$
$FeBr_2$	3.772	6.223	$P\bar{3}m$
$MnBr_2$	3.868	6.272	$P\bar{3}m$
Fe^{2+} 1.1%	3.661(2)	18.41(1)	$R\bar{3}m$
1.3%	3.660(2)	18.41(1)	$R\bar{3}m$
6.4%	3.703(14)	18.49(6)	$R\bar{3}m$
8.0%	3.662(3)	18.42(1)	$R\bar{3}m$
35%	3.679(4)	18.48(1)	$R\bar{3}m$
41%	3.712(11)	18.57(3)	$R\bar{3}m$
72%	3.745(5)	6.195(5)	$P\bar{3}m$
Mn^{2+} 3.3%	3.726(17)	18.54(7)	$R\bar{3}m$

Reflections in the powder neutron diffraction profiles of $NiBr_2$- and Fe^{2+}-doped samples were indexed according to the double hexagonal magnetic cell of the $CdCl_2$ structure. Values for the nuclear scattering lengths were taken from Ref. (*16*) and magnetic form factors for the Fe^{2+} and Ni^{2+} ions from the tables of Watson and Freeman (*17*). μ_{Fe} and μ_{Ni} were assigned the initial values 4.3 and 2.0 μ_B, respectively. These values are those giving the best fit to the magnetic neutron diffraction intensities in $NiBr_2$ (*3*) and $FeBr_2$ (*18*). The $FeBr_2$ moment was also confirmed by extrapolation

of the single-crystal magnetisation to 0 K (*19*). The neutron powder profiles were fitted by the Rietveld refinement method analysed using the POWDER suite of programmes mounted on the DEC 10 computer at the Edinburgh computing centre, accessed via the SERC interactive network.

The only positional parameter refined was the z coordinate u of the Br^- ion and the fractional occupation number of a metal ion site was fixed by the chemical composition. A collinear metamagnetic structure was assumed, though only the *KX* and *KZ* components of the moments were assigned, since their direction in a plane perpendicular to the unique z axis cannot be determined by the diffraction of unpolarised neutrons.

Tables II and III present the structural and magnetic parameters obtained from the refined profiles, together with the R values. The artificial enhancement of 001 reflections by the tendency of crystal platelets to stack with c axes parallel was compensated by the inclusion of a preferred orientation factor. A slight contraction of the lattice is evident from a comparison with the lattice constants measured at room temperature (Table I), as is the expansion introduced by increasing concentration of Fe^{2+}. u_{Br} consistently exceeds the value 0.125 appropriate to perfect octahedral coordination of the metal ions, which confirms the slight compression parallel to the trigonal z axis.

TABLE II

STRUCTURAL PARAMETERS OF Fe^{2+}-DOPED $NiBr_2$ SAMPLES FROM REFINEMENT OF THE POWDER NEUTRON DIFFRACTION PROFILES

Mole% Fe^{2+}	a_0 (Å)	c_0 (Å)	u_{Br}	R_{nucl}%	R_{magn}%
0	3.650	36.60	0.1277	4.31	17.6
8	3.658	36.66	0.1278	6.08	26.4
30	3.679	36.78	0.1271	9.70	36.3

Note. The double hexagonal magnetic cell is used. The R factors are included for comparison; R (magnetic) refers to the parameters in Table III.

TABLE III

THE COMPONENTS OF THE MOMENT OF THE ION AT THE (0,0,0) POSITION OF THE UNIT CELL, IN BOHR MAGNETONS ($\mu_{AV} = x_{Fe}\mu_{Fe} + x_{Ni}\mu_{Ni}$)

	μ_{Fe}			μ_{Ni}		
Mole% Fe^{2+}	*KX*	*KY*	*KZ*	*KX*	*KY*	*KZ*
0	—	—	—	2.0	0	0
8	4.2	0	0	2.0	0	0
30	0	0	4.2	0	0	2.0

The magnetic refinements are less well defined, though it is clear from the intensities of the 003_M and 009_M reflections that the moments lie to a close approximation within the *ab* plane in the $NiBr_2$ and 8%-Fe^{2+} structures but parallel to the c axis in the 30%-Fe^{2+} structure.

3.2. *Single-Crystal Neutron Diffraction*

Measurements of the 101_M and 003_M reflections were used to characterize the helical magnetic phases at 4.2 K. The magnitude and direction of the helix propagation vector τ is deduced from the distribution of satellites around the Bragg points, while by scaling the intensity of magnetic and nuclear reflections the average moment magnitude can be determined. In addition the temperature variation of τ is observed by following the collapse of the satellites towards the transition to the collinear magnetic phase at a temperature T_{IC}^9 and T_N from the variation of the total magnetic intensity. Finally, the ratio of the intensities of the 101_M and 003_M reflections is used to estimate the spin tilting angle ϕ. For the purposes of comparison of results obtained using different instruments, the effective detector tilt angle ν was scaled to a constant neutron wavelength of 1.1 Å, using the relation $(\sin \nu)/\lambda$ = constant. The scaled tilt angle is labelled ν'.

The results of diffraction by single crystals having a helical phase at 4.2 K are presented in Table IV and Figs. 1a–c. All dis-

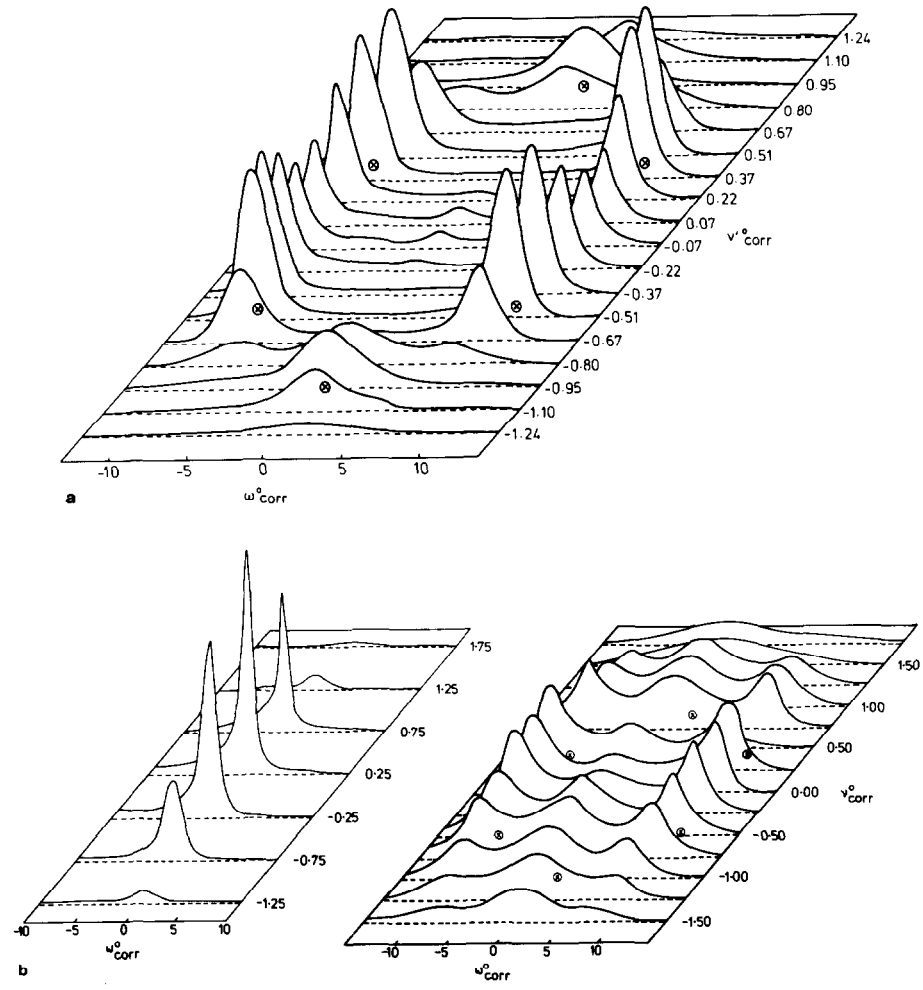

FIG. 1. Diffraction profiles of the 003_M reflection, for crystals exhibiting a helimagnetic phase. The data are presented in the form of perspective diagrams in the ω, ν' plane of detector space, where ν' is scaled to a neutron wavelength of 1.1 Å. The instruments employed, the crystal orientations and mosaic spreads and the measured propagation vectors are listed in Table IV. (a) Pure $NiBr_2$ at 6 K; (b) 2.0(4) mole% Fe^{2+} at 4.7 and 25 K; (c) 8.5 mole% Fe^{2+} at 4.6 and 28 K (inset).

play satellite hexagons in the **a*b*** plane, within which τ therefore lies. No satellites were found in scans parallel to **c***, and no higher-order satellites were observed during wider scans around 003_M nor was scattering found at 003_M, confirming that the modulations of the moments are sinusoidal. Although the crystals were cooled in the absence of a magnetic field, the populations of the three equivalent domains (judged from the relative intensities of diametrically opposed satellite pairs) were frequently observed to be unequal. This is probably due to stress within the crystals.

In Figs. 1a–c the intensity profiles of the 003_M reflections at 4.2 K for the crystals listed in Table IV are presented in the form of ω scans at fixed values of ν'. The satellites are broadened in the ν' direction as a consequence of the mosaic spread and the

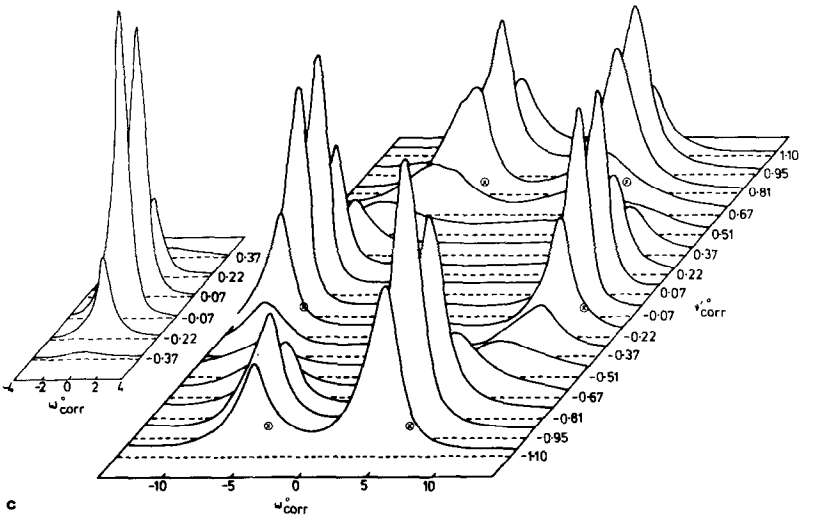

FIG. 1—*Continued.*

distortion imposed by the magnitude of the reflecting sphere radius on the scale of the 003_M scattering vector. This distortion is less significant at a neutron wavelength of 4.52 Å, and individual satellites are resolved in scans recorded on D16.

The crosses in Fig. 1 mark the satellite positions of a model structure with a propagation vector in the [110] or [100] direction in the a*b* plane. In most instances, helical phases with propagation vectors weighted in the [110] or [100] directions can be readily distinguished.

TABLE IV

PARAMETERS OF THE INCOMMENSURATE PHASES AT 4.2 K FROM SINGLE-CRYSTAL NEUTRON DIFFRACTION

Mole% dopant	Instrument	Mosaic ω^0	Spread ν'^0	τ (helix) Direction	τ (helix) 10^2 (Å^{-1})
Pure $NiBr_2$	D16	1.5	0.29	110	1.46(5)
Fe^{2+} 0.67	Mk.VI	2.0	—	110	1.47(5)
0.86	D15	1.2	0.6	110	1.47(4)
2.0(4)	Mk.VI	1.5	1.5	110	1.49(4)
5.3(8)	Mk.VI	1.3	1.5	100	1.49(4)
5.7	Mk.VI	1.5	1.3	100	1.51(4)
5.7(5)	Mk.VI	2.0	1.2	100	1.41(8)
6.1(16)	Mk.VI	1.5	1.2	100	1.49(4)
8.0	Mk.VI	1.6	1.4	100	1.50(4)
8.5	Mk.VI	1.2	1.1	100	1.50(4)
8.5	D16	1.2	0.28	100	1.51(2)
Mn^{2+} 2.4	Mk.VI	1.5	—	110	1.55(4)

Some scans of the 003_M reflection in the collinear magnetic phase above T_{IC} are included for comparison. They were recorded under the same experimental conditions as the scans of the satellites at 4.2 K. The helical propagation vector in pure $NiBr_2$ is in the [110] directions (Fig. 1). At 4.2 K, the wavelength of the modulation is 68.6 (23) Å or 38 (1) d_{110}. The moments therefore rotate by approximately 9.5° between adjacent (110) planes and the propagation vector is [0.026,0.026,0].

Within experimental error, the magnitude of τ in $Fe_xNi_{1-x}Br_2$ remains unchanged from the value in pure $NiBr_2$, up to $x = 0.085$. Samples with compositions $x = 0.11$ and $x = 0.31$ exhibit collinear, easy-axis magnetic structures down to the lowest temperature. A transition to this type of magnetic structure therefore occurs in the composition range $0.085 \leq x \leq 0.11$. On the other hand, in the composition range $0.020(4) \leq x \leq 0.053(8)$ the propagation vector direction changes from [110] to [100].

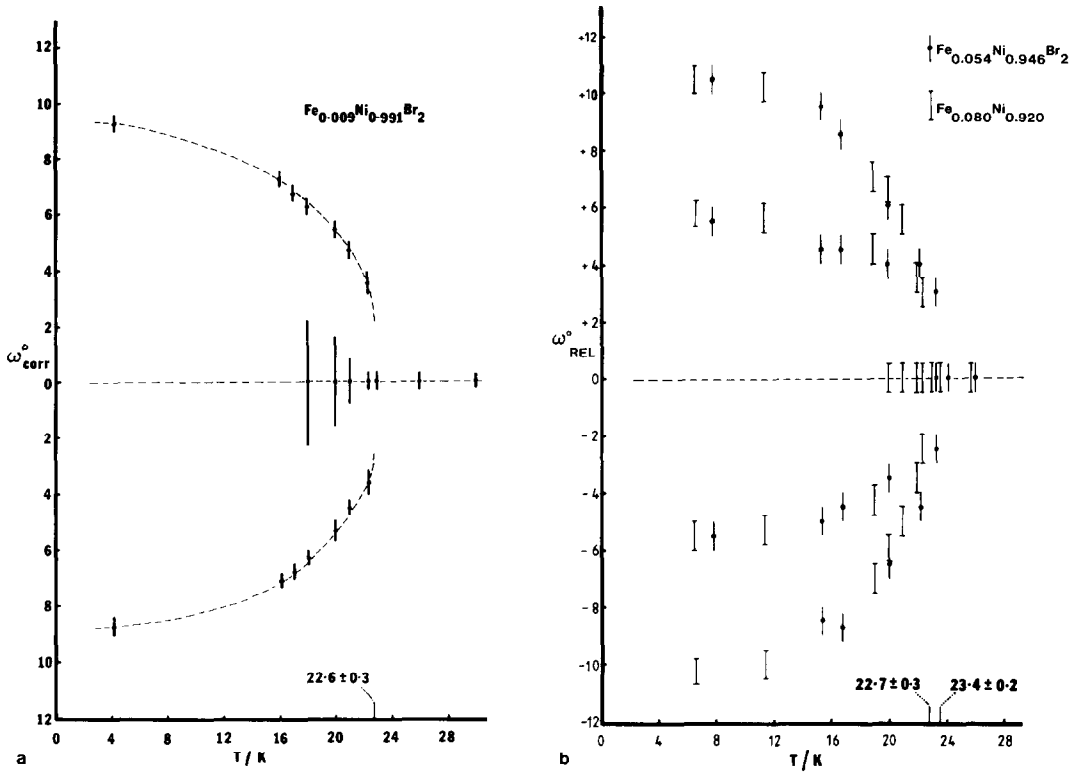

FIG. 2. Temperature dependence of the 003_M satellite separation for $Fe_xNi_{1-x}Br_2$ with (a) τ in the [110] direction and (b) τ in the [100] direction.

A single sample of $Mn_xNi_{1-x}Br_2$ with $x = 0.024$ exhibits a propagation vector in the same direction as pure $NiBr_2$, but of slightly increased magnitude.

The magnitude of τ_{110} decreases smoothly from its limiting value at 4.2 K as the temperature is increased (*3, 4*). At $T_{IC} \sim 23$ K, it collapses sharply to zero over a temperature range of approximately 1 K depending upon the instrumental resolution. Crystals doped with Zn^{2+} and Cl^- ions behave similarly (*8, 9*). To study the temperature dependence of τ in $M_xNi_{1-x}Br_2$ (M = Fe, Mn), crystals were aligned in the *h0l* scattering plane and ω scans through the 003_M Bragg position were performed at $\nu_{corr} = 0$. A narrow horizontal collimation of the diffracted beam maximised the resolution but the vertical divergence of the beam was not collimated, in order to maximise the collected intensity. The appearance of the scans depends on the direction of τ. When τ lies along [110], a single pair of peaks, which stem from the overlap of the domain pairs 1 and 2 is observed. When τ lies along [100], two pairs of equally spaced peaks, which arise from the overlap of the domain pairs 2 and 3, and the domain pair 1 are observed. Figures 2a and b show examples of each type. Unfortunately it is not possible to decide whether the intensity which appears at the central Bragg position originates from a true collinear antiferromagnetic component of the structure, or from the unresolved satellites. Values of T_{IC} obtained in this manner are listed in Table V. In addition the width of the phase transition (Δ) at T_{IC} can be measured by plotting the

TABLE V

MEASURED TRANSITION TEMPERATURES AND PROPAGATION VECTORS OF DOPED $NiBr_2$ CRYSTALS[a]

Mole% dopant	T_{IC} (K) (a)[b]	T_{IC} (K) (b)	T_N (K) (c)	T_N (K) (d)	τ_n (helix) Direction	τ_n (helix) 10^2 (Å^{-1})	Δ (K) (1)
Pure $NiBr_2$	22.5(5)	22.8(3)	44	—	110	1.46(5)	~1
Fe^{2+} 0.67	(28.2(3))	(27.5)	(51.2(8))	—	110	1.47(4)	1.5
0.86	—	22.6(3)	44.9(2)	—	110	1.47(4)	—
2.0(4)	22.2(8)	23.0(5)	43.5(5)	43.5(5)	110	1.49(4)	2
5.3(8)	23.5(5)	23.2(4)	44.4(7)	44.0(4)	100	1.49(4)	1
5.7	23.0(10)	23.5(5)	40.2(5)	40.2(5)	100	1.51(4)	2
5.7(5)	23.0(10)	23.0(5)	—	—	100	1.41(8)	2
6.1(16)	23.0(10)	23.0(3)	44.3(5)	43.0(2)	100	1.49(4)	2
8.00	—	22.7(3)	40.4(5)	—	100	1.50(4)	—
8.5	—	23.4(2)	39.4(2)	—	100	1.50(4)	—
11.2(3)	Collinear		28.5(15)	—		Collinear	
31.3	Collinear		24.7(3)	—		Collinear	
Mn^{2+} 2.4	22.0(5)	21.5(5)	45.2(5)	45.2(5)	110	1.55(4)	2

[a] Δ is the width of the transition at I_{IC}.

[b] (a) From intensity at $\omega_{corr} = 0$; (b) from satellite separation; (c) from $I^{int}_{003_M}$; (d) from $I^{max}_{003_M}$.

maximum intensity at the 003_M Bragg position against temperature. The results are listed in Table V, and Fig. 3 illustrates an example.

For $Fe_xNi_{1-x}Br_2$ T_{IC} remains unchanged from $x = 0$ up to the transition to the collinear, easy-axis magnetic structure between $x = 0.083$ and 0.11 even though τ changes from the [110] to the [100] direction in the composition range $0.02 \leq x \leq 0.053$. The width of the transition, Δ, increases slightly to 2 K, but it remains essentially first-order. A slight decrease in T_{IC}, to about 21.5(5) K, was observed for a crystal of $Mn_{0.024}Ni_{0.976}Br_2$ and the transition again remains first-order.

The three-dimensional antiferromagnetic ordering temperature T_N depends upon the magnitude of the antiferromagnetic interplanar exchange constant j'. T_N values of single crystals of the pure materials are approximately 44 K ($NiBr_2$), 11 K ($FeBr_2$), and 2.2 K ($MnBr_2$). To discover whether T_N changes as a result of doping, temperature dependence of 003_M was measured. In the easy-plane crystals the intensity of 101_M is usually too small to allow an accurate determination of the magnetisation curve, but this proved to be possible for one crystal of $Fe_xNi_{1-x}Br_2$. Data were measured without any collimation of the detected beam, to ensure that below T_{IC}, all the intensity at satellite positions was collected.

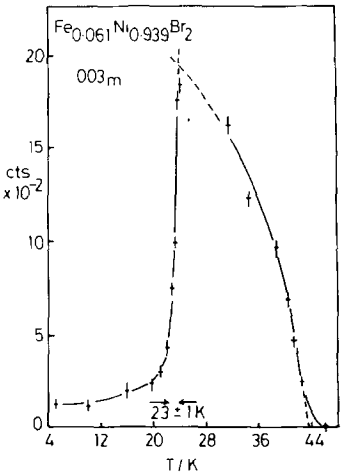

FIG. 3. Temperature dependence of the maximum intensity at 003_M for a $NiBr_2$ crystal containing 6.1(16) mole% Fe^{2+}.

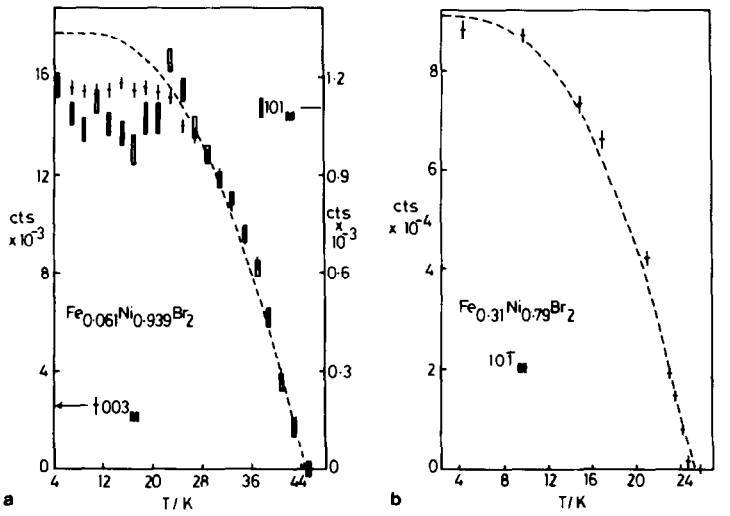

FIG. 4. Magnetisation curves of Fe^{2+}-doped $NiBr_2$ crystals. The integrated intensity of the named reflection is plotted against temperature, and the dotted lines are the best fits to a $S = 1$ Brillouin curve. (a) 6.1(16) mole% Fe^{2+}; (b) 31.3 mole% Fe^{2+}.

Figures 4a and b illustrate some of the measured magnetisation curves, where the dotted lines represent $S = 1$ mean field Brillouin plots. The values of T_N are listed in Table V. The crystals which have helical magnetic phases at low temperature all display T_N values close to that of $NiBr_2$.

Above the critical concentration of Fe^{2+} ions at which a transition to the collinear, easy-axis magnetic structure occurs, T_N falls rapidly towards the value of 11 K measured for $FeBr_2$ and the magnetisation curves of crystals containing 11.2 and 31.3% Fe^{2+} follow the mean field curve closely over the entire temperature range (Fig. 4).

The magnitude of the average ionic moment is calculated by comparing the intensities of magnetic and nuclear reflections. Table VI lists the values of the mean saturation magnetic moment, μ, determined in this manner. μ was determined from the intensity of magnetic reflections at 4 K and from the intensities provided by extrapolation of the Brillouin curves to 4 K. Taking the values of μ_{Fe} and μ_{Ni} from those which give the best fit to the neutron diffraction data on the pure bromides (*3*, *18*), $\mu_{MODEL} = 4.3x_{Fe} + 2.0x_{Ni}$ if the Fe^{2+} and Ni^{2+} moments are assumed to be collinear. 006_N, 0012_N, 102_N, and 104_N nuclear reflections were chosen for the scaling. μ_{Br} and the tilt angle ϕ were allowed to vary until the most consistent value of μ had been obtained. It can be seen that the observed values of μ are consistently less than μ_{MODEL}, even allowing for the dips in the magnetisation curves below T_{IC} which some samples exhibited.

TABLE VI

MEASURED VALUES OF THE MEAN SATURATION MOMENT, μ, IN $Fe_xNi_{1-x}Br_2$ (IN BOHR MAGNETONS)

Mole% dopant (Fe^{2+})	μ_{Br}	Reflection	ϕ^0	μ_{MODEL}	μ_{OBS}
0.86	0.125	003_M	90	2.0	1.60(12)
	0.127	003_M	90	2.0	1.80(12)
2.0(4)	0.126	003_M	90	2.0	1.74(10)
5.7	0.126	003_M	90	2.0	1.76(60)
6.1(16)	0.125	003_M	90	2.0	1.56(8)
	0.125	101_M	90	2.0	1.46(12)
11.2	0.126	101_M	0	2.2	1.92(14)
31.3	0.127	101_M	0	2.8	2.4(2)

3.3. *Optical Absorption Spectra*

The broad features of the absorption spectra of the Fe- and Mn-doped crystals between 5800 and 6100 Å are similar to that of $NiBr_2$, though there are significant changes of detail. Figure 5 displays the spectrum of a 0.6% Fe^{2+} crystal in the region 6050 to 6110 Å as a function of temperature, and the details of the hot and cold band structure of all the crystals are recorded in Table VII.

The cold bands of the Fe- and Mn-doped samples at 5 K are compared with that of $NiBr_2$ in Fig. 6. In each case, a smooth decrease in the intensity up to T_{IC} was observed. The positions of the cold bands remained constant in all the spectra.

In all the doped crystals there are hot bands such as those labelled CC' in Fig. 5. Since they were found to be independent of applied magnetic field, their intensity was measured in the presence of a field H_{ab} H_{cnt}, sufficient to remove the cold band structure. The positions and intensities of the hot bands C,C′ are listed for all samples in Table VII. Only in $NiBr_2$ is there a discontinuity in intensity at T_{IC}, when a transition from T^3 to T^2 behaviour occurs. Increasing dopant concentration reduces n in the T^n law below the value of 2 which is expected when the planar anisotropy constant is small, relative to J_1.

TABLE VII

THE CHARACTERISTICS OF COMBINATION BANDS APPEARING IN THE AXIAL SPECTRA OF $NiBr_2$ SYSTEMS

Mole% dopant		λ (Å)	FWHM[a] (Å)	Peak OD (mm^{-1})	Temperature dependence	Label
Pure $NiBr_2$		6070	~8	~0.4(30 K)	hot	C
		6077	~8	~0.35(30 K)	hot	C′
		6080.2	1	0.12(4 K)	cold	B
		6082.9	1	0.60(4 K)	cold	B′
Fe^{2+}	0.6	6069	~8	~0.35(30 K)	hot	C
		6077	~8	~0.35(30 K)	hot	C′
		6080.0	2.5	040(4 K)	cold	B
		6084.5	2.5	0.28(4 K)	cold	A
	0.8	6070	—	~0.4(30 K)	hot	C
		6076	—	0.5(30 K)	hot	C′
		6081	~3	0.28(4 K)	cold	B
		6084.5	~3	0.42(4 K)	cold	A
		6097	~3	0.05(4 K)	cold	D
	11	6080	~20	~0.4(30 K)	hot	C, C′
		6085	—	—	cold	A
		6095	~10	~0.2(4 K)	cold	D
	23	6075	~20	—	hot	C, C′
			no cold bands			
Mn^{2+}	2.9	6071	~8	~0.35(30 K)	hot	C
		6079	~8	~0.35(30 K)	hot	C′
		6080(1)	3	0.01(4 K)	cold	B
		6083	~3	~0.4(4 K)	cold	B′

[a] Full width at half-maximum intensity.

A magnetic field applied in the basal plane of an easy-plane helimagnet such as

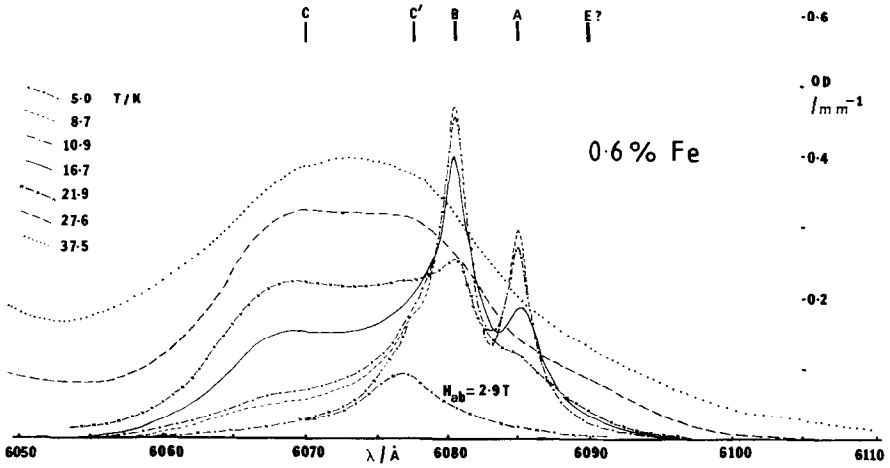

FIG. 5. Temperature dependence of the axial absorption spectrum of a $NiBr_2$ crystal containing 0.6 mole% Fe^{2+} (6050 to 6110 Å).

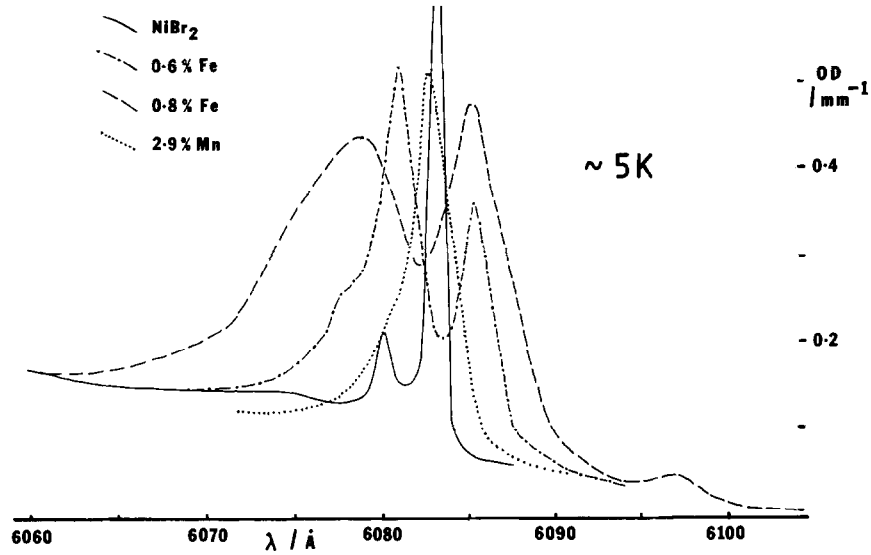

FIG. 6. Comparison of the cold band envelopes in the absorption spectra of pure and doped $NiBr_2$ crystals at 5 K.

$NiBr_2$ induces a first-order transition to a collinear phase (*8*). The intensity of the cold bands remains constant up to this value of the applied field, then falls to zero over a range of about 0.2 T, as illustrated in Fig. 7 for a crystal containing 2.9 mole% Mn. The intensities are normalised to unity at zero field, and the critical field is taken to be the value ($H_{1/2}$) at which the intensity is halved. A plot of $H_{1/2}$ against T yields the phase diagram in the (H_{ab},T) plane shown in Fig. 7b. The spin flop transitions were very sharp for all the samples studied, which suggests that concentration gradients in the doped crystals are small, and the pronounced hysteresis observed when increasing or decreasing the field confirms that the transition is of first-order. For the 2.9

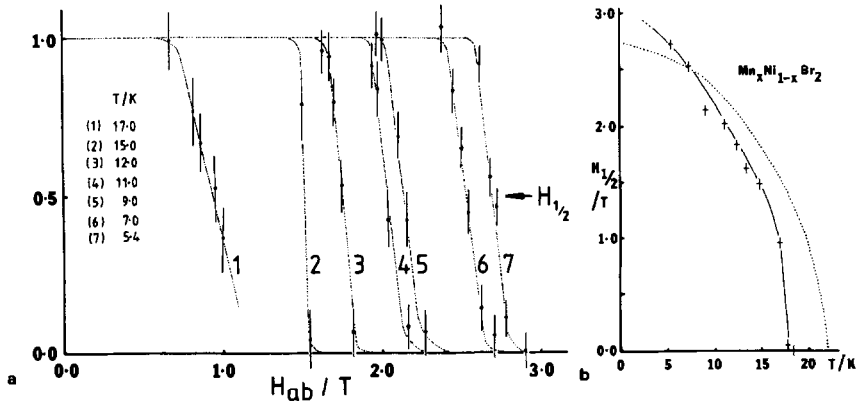

FIG. 7. (a) The variation of cold band intensity with magnetic field applied in the basal plane, for a $NiBr_2$ crystal containing 2.9 mole% Mn^{2+}, showing how $H_{1/2}$ is defined; (b) the derived (H_{ab},T) phase diagram (broken line $NiBr_2$).

mole% Mn-doped crystal we find $H_{1/2}$ = 3.0 T and T_{IC} = 17.8(4) K compared with $H_{1/2}$ = 2.7 T and T_{IC} = 22.0(4) K for $NiBr_2$.

The complete phase diagram of $Fe_xNi_{1-x}Br_2$ could not be measured because the cold bands are rapidly dominated by the growing hot bands as the temperature is increased. At 5 K, samples containing 0.6 and 0.8 mole% Fe exhibited a critical field $H_{1/2}$ = 2.70(2) T. Since both these samples also exhibit T_{IC} values close to that of pure $NiBr^2$ it appears that their phase diagrams closely resemble that of the pure material.

4. Discussion

4.1. Magnetic Phase Diagram and Magnetisation

Figure 8 shows the magnetic phase diagram of $Fe_xNi_{1-x}Br_2$ in the (x,T) plane obtained from our neutron diffraction measurements (the phase labels are those of Rastelli *et al.* (*5*)). Despite a continuous decrease of τ with increasing temperature, the helical and collinear phases coexist over a small temperature range near T_{IC}, so that IV, III $\leftrightarrow$ I transitions are believed to be first order. In this conclusion we agree with Adam *et al.* (*7*) though it should be noted

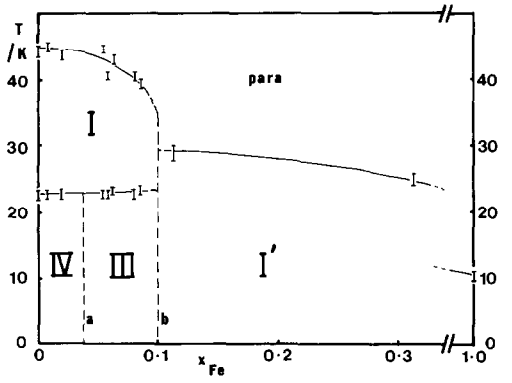

FIG. 8. Magnetic phase diagram of the $Fe_xNi_{1-x}Br_2$ system in the (x,T) plane, from neutron diffraction measurements.

that simultaneous observation of commensurate and incommensurate features does not automatically lead to this conclusion since strain, or kinetic effects may pin some parts of the crystal in the commensurate phase. Since the τ direction is sharply defined in all $Fe_xNi_{1-x}Br_2$ systems ($x \leq 0.085$) the transition between helical phases III and IV is also believed to be first order in x.

Ito *et al.* (*20*) determined the magnetic phase diagram of the closely related $Fe_xNi_{1-x}Cl_2$ from the temperature dependence of 101_M and 003_M reflections. Although the competition between the single ion anisotropies of Fe^{2+} and Ni^{2+} is similar to that in $Fe_xNi_{1-x}Br_2$, the exchange competition is not sufficient to establish a helimagnetic phase. For compositions $x \geq 0.12$, the dominant axial anisotropy of the Fe^{2+} ions orders all moments parallel to the c axis below T_N. For compositions $0.005 \leq x \leq 0.12$, long-range order is first established in the component in the *ab* plane, but below a temperature T_L the moments tilt out of the plane by an increasing degree. For example, the angle between the mean moment direction and the c axis reaches a limiting value of 30° at 4.2 K in the $x \sim 0.06$ sample. T_L decreases with decreasing Fe^{2+} concentration such that no canted phase exists below $x \sim 0.005$.

Contrary to expectations, the $Fe_xNi_{1-x}Br_2$ system does not exhibit a canted phase of this type, unless it is confined to the narrow composition range $0.085 \leq x \leq 0.11$. Our diffraction experiments are not sufficiently sensitive to determine the orientation of the Fe^{2+} moments in the range $0 \leq x \leq 0.1$, but the Ni^{2+} moments order in the *ab* plane in this range.

We may speculate on the existence of multicritical points on the phase diagram. For example, in the region of $x \sim 0.1$ in the $Fe_xNi_{1-x}Br_2$ phase diagram one could envisage a coexistence of the two collinear magnetic phases (I, I') with either the paramagnetic or the helical phase (III). A simi-

lar point exists on the $Fe_xNi_{1-x}Cl_2$ phase diagram close to $x = 0.12$.

Below T_{IC} the temperature dependence of the spontaneous magnetisation deviates quite markedly from that calculated using a molecular field model (Fig. 4a). Significantly, antiferromagnetic resonance measurements on $NiBr_2$ have shown that, when a magnetic field less than the critical value 2.7 T is applied in the *ab* plane, *g* increases continuously from 2.06(2) at 10 K to 2.27 at T_{IC} (*21*). Similarly, magnetisation measurements in a field applied in the *ab* plane show that, at temperatures below T_{IC}, the magnetisation increases suddenly when the transition to the collinear phase takes place (*22*).

However, even when the reduction in the magnetisation below T_{IC} is taken into account, the values of the saturation moment determined from our neutron scattering measurements are frequently well below the calculated spin-only values (Table VI). If the nuclear reflections used in the scaling procedure were subject to extinction or absorption effects, the measured moments would be too large. For comparison the values of the saturation moment of the Ni^{2+} ion in nickel halides determined from neutron diffraction measurements are

$2.24\mu_B$	$NiCl_2$,	Ref. (*23*)
$2.00(15)\mu_B$	$NiBr_2$,	Ref. (*3*)
$1.56\mu_B$	NiI_2,	Ref. (*24*)

These may be compared with the spin-only value of $2.0\mu_B$ ($S = 1$). An orbital contribution must derive from spin orbit coupling in second order, because the $^3A_{2g}$ ground state of the Ni^{2+} ion has zero orbital angular momentum.

4.2. Relation to the (j_2,j_3) Magnetic Phase Diagram

Table VIII summarises the exchange and anisotropy constants of $NiBr_2$ at 4.2 K reexpressed in the form of ratios $j_n = z_nJ_n/z_1J_1$ in order to relate them to the theoretical phase diagram in the (j_2,j_3) plane. A comparison is also made with the measured exchange constants of the metamagnets $NiCl_2$ (*23*), $FeBr_2$ (*25*), $FeCl_2$ (*26*), $CoBr_2$ (*27*), and $CoCl_2$ (*28*). No measurements on the iodides have been reported, although a mean field calculation on NiI_2 gives $J_1 = 0.32$ THz, $J_2 = -0.14$ THz ($j_2 = -0{,}44$) (*24*).

Comparing the bromides and chlorides of the same transition metal, j'(bromide) $\sim 3j'$(chloride) and d(bromide) $\geq d$(chloride). However, the most striking difference is the increased magnitude of J_3 in $CoBr_2$ and $NiBr_2$ compared with the corresponding chlorides, which is responsible for the low-temperature helimagnetic phase in the latter case. j_3 was neglected in the analysis of the $NiCl_2$ spin wave dispersion curves (*23*), so it would be illuminating to measure the dispersion in the $[q,q,0]$ direction to discover whether j_3 is indeed small. j_2 does not vary in a monotonic fashion with the atomic number of the cation, either in the chlorides or bromides.

Figure 9 shows the region close to the origin of the (j_2,j_3) phase diagram calculated by Rastelli *et al.* for a two-dimensional hexagonal Heisenberg magnet (*5*), on which the boundary between phases I and IV has been shifted slightly by the inclusion of the measured value of j'. Along the broken line in the helical phase regions the magnitude of τ is constant. If $a\tau$ is the reduced propagation vector magnitude, the equations of these lines are (*5*):

Phase III, $\tau[100]$

$$1 + j_2 - j'/3 + 2(j_2 + 2j_3)\cos X = 0 \quad (1)$$

where the turn angle X between adjacent (100) planes is $\sqrt{3}\pi a\tau$.

Phase IV, $\tau[110]$

$$1 - 3j_2 - j' + 2(1 - 2j_3)\cos Y + 12j_2\cos^2 Y + 16j_3\cos^3 Y = 0 \quad (2)$$

TABLE VIII

EXCHANGE AND ANISOTROPY CONSTANTS OF METAMAGNETIC TRANSITION METAL CHLORIDES AND BROMIDES, DETERMINED AT 4.2 K BY INELASTIC NEUTRON SCATTERING

Material	J_1 (THz)	j_2	j_3	j'	d	Ref.
$NiBr_2$	0.379(1)	0.011(13)	−0.277(14)	−0.119(6)	0.095(13)	(33)
$NiBr_2$	0.377(5)	−0.012(13)	−0.263(16)	−0.117(5)	0.052(33)	(34)
$NiCl_2$	0.451	−0.224	—	−0.033	0.018	(23)
$FeBr_2$	0.152(8)	−0.339(57)	—	−0.13(2)	−1.46(21)	(25)
$FeCl_2$	0.164(5)	−0.125(35)	—	−0.044(15)	−1.28(15)	(26)
$CoBr_2$	0.482(3)	0.01(3)	−0.168(4)	−0.161(3)	0.567(8)	(27)
$CoCl_2$	0.593(6)	—	—	−0.076(6)	0.56(6)	(28)

Note. $J_n = z_nJ_n/z_1J_1$, where z_n is the number of neighbours in the nth coordination sphere.

where the turn angle Y between adjacent (110) planes is $\pi a\tau$.

On the boundary with the easy-plane collinear phase I, $X = Y = 0$ and Eqs. (1) and (2) reduce to

$$1 + 3j_2 + 4j_3 - j'/3 = 0. \qquad (3)$$

When $NiBr_2$ is doped with Fe^{2+} the large axial single ion anisotropy constant of Fe^{2+} ($d(FeBr_2)/d(NiBr_2) = -15$) constrains all moments to lie parallel to the c axis above a limiting concentration $x_{Fe} = \sim 0.1$. At lower Fe^{2+} concentrations, the magnitude of the propagation vector τ which characterises the helical phase at 4.2 K ($a\tau = 0.054(2)$) is unchanged from that of pure $NiBr_2$ ($a\tau = 0.053(2)$) but a transition from phase IV to phase III takes place in the composition range $0.020 \leq x_{Fe} \leq 0.053$.

The Fe^{2+}-doped systems therefore lie on

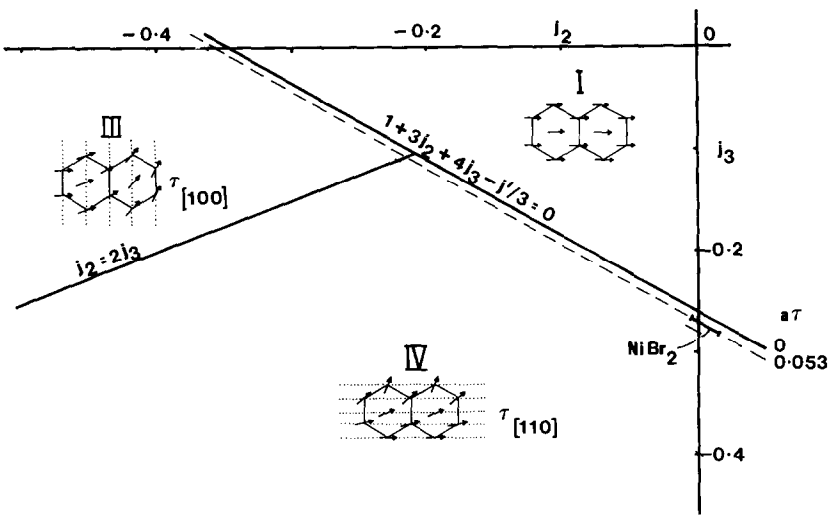

FIG. 9. Phase diagram of the easy-plane hexagonal Heisenberg magnet at 0 K (5). j' takes the value −0.119 measured for $NiBr_2$ and the reduced propagation vector magnitude, $a\tau$, is constant on the broken line $a\tau = 0.053$ ($NiBr_2$ and $Fe_xNi_{1-x}Br_2$).

the line of constant τ appropriate to $NiBr_2$ (Fig. 9). From Eqs. (1) and (2) and taking j' to be -0.119 as in the pure bromide

$$2.87j_2 + 3.77j_3 + 1 = 0. \quad (4)$$

If we apply the constraints $j_2 \geq 2j_3$ (phase IV) or $j_2 \leq 2j_3$ (phase III), then

$$j_2 \geq -0.210; \quad j_3 \leq -0.105 \quad \text{(phase IV)}$$

$$j_2 \leq -0.210; \quad j_3 \leq -0.105 \quad \text{(phase III)}$$

to be compared with

$$j_2 = +0.011(13); \quad j_3 = -0.277(14) \quad (NiBr_2, \text{ phase IV}).$$

Thus assuming that there is no change in the Ni^{2+} anisotropy constant on doping Fe^{2+} into $NiBr_2$ a comparatively large increase in j_3 and decrease in j_2 with increasing Fe^{2+} concentration is required to reproduce the observed behaviour. Perturbations of the local exchange environment rather than the very small lattice expansion are almost certainly responsible, since the latter would increase τ and T_{IC} while leaving the direction of τ unchanged. That T_{IC} remains unchanged from the $NiBr_2$ value is consistent with the supposition that all $Fe_xNi_{1-x}Br_2$ systems (up to $x = 0.085$) lie on a line of constant τ parallel to the boundary with the collinear phase (j' should not be affected by cation doping).

The transition from phase IV to phase III occurs sharply with increasing Fe^{2+} concentration (τ is strongly weighted in the [110] and [100] directions in the 2.0% Fe^{2+} and 5.3% Fe^{2+} crystals, respectively). Transitions between helical phases III and IV on the line $j_2 = 2j_3$ should indeed be first order.

τ and T_{IC} remain virtually unchanged when 2.4 mole% Mn^{2+} is present in the lattice, which in turn suggests that the fluctuations of the local exchange environment are also small. Studies over a wider composition range will be necessary to discover whether the behaviour is indeed similar to the $Zn_xNi_{1-x}Br_2$ system (the Mn^{2+} ion approximates to a diamagnetic dopant since the magnitudes of the exchange constants in $MnBr_2$ are small compared to $NiBr_2$).

Finally, no disordering of the propagation vector direction in the **a*b*** plane was observed in any of the $Fe_xNi_{1-x}Br_2$ crystals. Behaviour of this sort would be expected if a system lies close to the boundary between helical phases III and IV. Rastelli *et al.* have shown (*29*) that on this line there are an infinite number of degenerate helices whose wave vector τ satisfy the conditions

$$-\cos(\pi\sqrt{3}a\tau_x) = \frac{1 - 3j_2 + 4j_2\cos^2(\pi a\tau_y)}{4j_2\cos^2(\pi a\tau)_y}$$

and

$$\tau_z = 0$$

describing a circle around the Bragg point. Such a mechanism has been proposed to explain the isotropic helimagnetic phase of a crystal containing 7.7% Zn^{2+} (*8*), but crystal inhomogeneity cannot be ruled out.

4.3. Optical Spectra

In $Fe_xNi_{1-x}Br_2$ and $Mn_xNi_{1-x}Br_2$ no single ion transitions of the dopant ion occur in the region 5800 to 6100 Å, where the effects of magnetic interactions on spin-forbidden transitions of the nickel ions are observed. Any perturbations of the local exchange field around the nickel ions should therefore be observable.

The cold bands A and B in Fig. 5 are characteristic of the helical phase, collapsing smoothly, with no change in energy, with increasing temperature, to disappear at 23.0(10) K (0.6 mole% Fe^{2+}) and 23.3(7) K (0.8 mole% Fe^{2+}), in accord with the values of T_{IC} measured by neutron diffraction. They are also removed completely above a critical field applied in the *ab* plane. They therefore arise from two sharp maxima in

the density of magnon states associated with the in-plane magnon dispersion near $\mathbf{k} = \tau_{110}$, as discussed for pure $NiBr_2$ (*35*). The presence of Fe^{2+} ions within the lattice evidently changes the shape of the in-plane dispersion curves: the intensity ratio $I(A)/I(B)$ increases with increasing impurity ion concentration, until only band A is visible in the broad spectrum of a sample containing 11 mole% Fe^{2+}.

A new cold band, labelled D in Fig. 5, occurs at 6095 to 6097 Å, increasing rapidly in intensity with increasing concentration of Fe^{2+} ions. Both A and D may arise from essentially localised Fe^{2+}–Ni^{2+} pair transitions, but only if the Fe^{2-}–Ni^{2+} exchange is antiferromagnetic, and if the Fe^{2+} moments adopt an easy-plane configuration when diluted in the $NiBr_2$ lattice, as in the $Fe_xNi_{1-x}Cl_2$ case (*20*). Unfortunately our neutron diffraction measurements on $NiBr_2$ crystals containing less than 8.5 mole% Fe^{2+} were not sensitive enough to test this hypothesis.

The behaviour of the hot bands, labelled C and C′ in Fig. 5 is qualitatively very similar to pure $NiBr_2$, and they again stem from a ferromagnetic coupling component within the *ab* plane which is almost independent of the helical modulation. However, the intensity variation with temperature is less steep, and an exponent of 1.0(1) was measured for samples containing 0.6 and 0.8 mole% Fe^{2+}. This may be compared with the value 1.0 obtained (*30*) for a sample containing 7.7% Zn^{2+}, and the values 2.0, 1.3, and 0.7 obtained for samples containing 2, 5, and 10% $NiCl_2$, respectively (*31*). However, the spectra of samples containing 0.6 and 0.8% Fe^{2+} display a new band within the hot band manifold, which is independent of a magnetic field within the *ab* plane. Its intensity increases by a factor of about 1.5 as the Fe^{2+} concentration increases from 0.6 to 0.8 mole%, which is consistent with an absorption arising from Fe^{2+}–Ni^{2+} pairs, and it dominates the spectrum of a sample containing 11% Fe^{2+}. If this band is temperature independent the intensity of the hot band manifold would indeed appear to increase less steeply with increasing temperature since the two band systems overlap. Wood *et al.* (*32*) accounted for temperature-independent satellite bands to the main exciton–magnon combination in the spectra of $Rb_2Mn_xCr_{1-x}Cl_4$ samples by proposing transitions with antiferromagnetically coupled Mn^{2+}–Cr^{2+} pairs in the exchange field of the surrounding lattice and it is proposed that a similar mechanism operates in the present case.

The broad, overlapping hot and cold band structure prevented the determination of the phase diagram in the (H_{ab},T) plane by optical methods. However, measurements of the critical field required to effect a transition to the collinear phase were made at 5 K, when the cold bands are most intense. A value of 2.7(2) T was obtained for samples containing 0.6 and 0.8% Fe^{2+}, to be compared with 2.65(1) T for pure $NiBr_2$. Since T_{IC} is also unchanged, it appears that the phase boundary separating the helical and collinear phases has not moved. The transition remains first-order in field, which strongly implies that the broadening of the cold bands does not originate from concentration gradients within the samples, but rather from a broadening of the maxima in the density of magnon states.

A crystal containing 23% Fe^{2+} exhibited no cold bands in the region 6050 to 6100 Å. This is to be expected since our neutron diffraction experiments have shown that a sample of this composition adopts an easy-axis magnetic structure at all temperatures below T_N. A very broad hot band was still observed, although the in-plane magnon dispersion is expected to be rather different for a material with a large axial anisotropy constant.

An Mn^{2+}-doped crystal of $NiBr_2$ exhibits a single, broad asymmetric cold band con-

sisting of two components (B and B′ in Table VII), which correspond closely to the cold bands in pure $NiBr_2$. A comparison may be drawn with the single asymmetric cold band observed in the spectra of Zn^{2+}-doped samples (*30*). No new bands appear in the spectrum, and one may speculate that the Mn^{2+}–Ni^{2+} exchange constant is so small that the Mn^{2+} ions behave effectively as a diamagnetic diluent. The transition temperature T_{IC} is also reduced to 18.6(4) K which further supports the analogy with the $Zn_xNi_{1-x}Br_2$ system. If the dopant ions merely block exchange between Ni^{2+} ions the existence region of the helical phase on the (H_{ab},T) phase diagram should be reduced, as is observed for $Zn_xNi_{1-x}Br_2$. However, the phase diagram of the Mn^{2+}-doped sample shows a slight increase in the critical field extrapolated to 0 K. The hot bands C and C′ occur at the same wavelength as in pure $NiBr_2$, and they follow an intensity variation close to T^2 up to 30 K, as predicted for an easy-plane two-dimensional ferromagnet, with small planar anisotropy.

Acknowledgments

We acknowledge financial support from the U.K. Science and Engineering Research Council and thank the Atomic Energy Authority and Institut Laue–Langevin (ILL) for access to neutron beams. We are grateful to the University Support Group at Harwell and Dr. K. R. A. Zîebeck at the ILL for their help with the neutron diffraction experiments, to Dr. T. E. Wood for help with the optical spectroscopy, and to Dr. C. Wilkinson for valuable discussions.

References

1. K. KATSUMATA AND M. DATE, *J. Phys. Soc. Japan* **29,** 1090 (1971).
2. M. MORIMOTO AND M. DATE, *J. Phys. Soc. Japan* **29,** 1090 (1971).
3. A. ADAM, D. BILLEREY, C. TERRIER, R. MAINARD, L. P. REGNAULT, J. ROSSAT-MIGNOD, AND P. MERIEL, *Solid State Commun.* **35,** 1 (1980).
4. P. DAY AND K. R. A. ZIEBECK, *J. Phys. C* **13,** L523 (1980).
5. E. RASTELLI, A. TASSI, AND L. REATTO, *Physica B (Amsterdam)* **97,** 1 (1979).
6. P. DAY AND C. VETTIER, *J. Phys. C* **14,** L195 (1981).
7. A. ADAM, D. BILLEREY, C. TERRIER, H. BARTHOLIN, L. P. REGNAULT, AND J. ROSSA-MIGNOD, *Phys. Lett, A* **84,** 24 (1981).
8. P. DAY, M. W. MOORE, C. WILKINSON, AND K. R. A. ZIEBECK, *J. Phys. C* **14,** 3423 (1981).
9. P. DAY, K. J. TURNER, D. VISSER, AND T. E. WOOD, *Phys. Status Solidi B* **113,** 623 (1982).
10. P. DAY, A. T. DINSDALE, E. R. KRAUSZ, AND D. J. ROBBINS, *J. Phys. C* **9,** 2481 (1976).
11. P. GIORDANO, I. POLLINI, L. REATTO, AND G. SPINOLO, *Phys. Rev. B* **17,** 257 (1978).
12. M. KOZIELSKI, I. POLLINI, AND G. SPINOLO, *J. Phys. C* **5,** 1253 (1972).
13. D. J. ROBBINS AND P. DAY, *J. Phys. C* **9,** 867 (1976).
14. R. J. POLLARD, V. H. MCCANN, AND J. B. WARD, *J. Phys. C* **15,** 6807 (1982).
15. S. LEGRAND, *J. Cryst. Growth* **35,** 208 (1976).
16. G. E. BACON, "Neutron Diffraction," 2nd ed., Oxford Univ. Press (Clarendon), Oxford/New York, 1962.
17. R. E. WATSON AND A. J. FREEMAN, *Phys. Rev. Lett.* **6,** 277 (1961).
18. M. WILKINSON, J. W. CABLE, E. O. WOLLAN, AND W. C. KOEHLER, *Phys. Rev.* **113,** 497 (1959).
19. I. S. JACOBS AND P. E. LAWRENCE, *J. Appl. Phys.* **35,** 996 (1964).
20. A. ITO, T. TAMAKI, Y. SOMEYA, AND H. IKEDA, *Physica B* **120,** 207 (1983).
21. A. ADAM, D. BILLEREY, C. TERRIER, K. KATSUMATA, J. MAGARINO, AND J. TUCHENDLER, *J. Phys. Lett. A* **79,** 353 (1980).
22. K. KATSUMATA, K. SUGIYAMA, AND M. DATE, *J. Phys. Soc. Japan* **52,** 3312 (1983).
23. P. A. LINDGARD, R. J. BIRGENEAU, J. ALS-NIELSEN, AND H. J. GUGGENHEIM, *J. Phys. C* **8,** 1059 (1975).
24. S. R. KUINDERSMA, thesis, Groningen, 1980.
25. C. VETTIER, AND W. B. YELON, *J. Phys. C* **8,** 2760 (1975).
26. R. J. BIRGENEAU, W. B. YELON, E. COHEN, AND J. MAKOVSKY, *Phys. Rev. B* **5,** 2607 (1972).
27. H. YOSHIZAWA, K. UBUKOSHI, AND K. HIRAKAWA, *J. Phys. Soc. Japan* **48,** 42 (1980).
28. M. T. HUTCHINGS, *J. Phys. C* **6,** 3143 (1973).
29. E. RASTELLI, L. REATTO, AND A. TASSI, *J. Phys. C* **16,** L331 (1983).
30. M. W. MOORE, Chemistry Part II thesis, Oxford, 1980.

31. P. DAY, K. J. TURNER, D. VISSER, AND T. E. WOOD, *Phys. Status Solidi B* **113,** 623 (1982).

32. T. E. WOOD, P. A. COX, AND P. DAY, *J. Phys. C* **15,** L787 (1982).

33. P. DAY, M. W. MOORE, T. E. WOOD, D. MCK. PAUL, K. R. A. ZIEBECK, L. P. REGNAULT, AND J. ROSSAT-MIGNOD, *Solid State Commun.* **51,** 627 (1984).

34. L. P. REGNAULT, J. ROSSAT-MIGNOD, A. ADAM, D. BILLEREY, AND C. TERRIER, *J. Phys. (Orsay, Fr.)* **43,** 1283 (1982).

35. M. W. MOORE, T. E. WOOD, AND P. DAY, *J. Chem. Soc. Faraday Trans. 2* **77,** 1611 (1981).